ACSNANO

www.acsnano.org

ARTICLE

Enhanced Photovoltaic Performances of La-Doped Bismuth Ferrite/Zinc Oxide Heterojunction by Coupling Piezo-Phototronic Effect and Ferroelectricity

Yuanzheng Zhang,[⊥] Liya Yang,[⊥] Yaju Zhang, Zhenyu Ding, Mengjun Wu, Yan Zhou, Chunli Diao, Haiwu Zheng,* Xingfu Wang,* and Zhong Lin Wang*

Cite This: *ACS Nano* 2020, 14, 10723−10732

Read Online

ACCESS | Metrics & More | Article Recommendations | Supporting Information

ABSTRACT: **Ferroelectric materials have drawn widespread attention due to their switchable spontaneous polarization and anomalous photovoltaic effect. The coupling between ferroelectricity and the piezo-phototronic effect may lead to the design of distinctive photoelectric devices with multifunctional features. Here, we report an enhancement of the photovoltaic performances in the ferroelectric *p*-type La-doped bismuth ferrite film (BLFO)/*n*-type zinc oxide (ZnO) nanowire array heterojunction by rationally coupling the strain-induced piezoelectricity in ZnO nanowires and the ferroelectricity in BLFO. Under a compressive strain of −2.3% and a 10 V upward poling of the BLFO, the open-circuit voltage (V_{OC}) and short-circuit current density (J_{SC}) of the device increase by 8.4% and 54.7%, respectively. Meanwhile, the rise (/decay) time is modulated from 153.7 (/108.8) to 61.28 (/74.86) ms. Systematical band diagram analysis reveals that the promotion of photogenerated carriers and boost of the photovoltaic performances of the device can be attributed to the modulated carrier transport behaviors at the BLFO/ZnO interface and the superposed driving forces arising from the adding up of the piezoelectric potential and ferroelectric polarization. In addition, COMSOL simulation results of piezopotential distribution in ZnO nanowire arrays and the energy band structure change of the heterojunction further confirm the mechanisms. This work not only presents an approach to design high-performance ferroelectric photovoltaic devices but also further broadens the research scope of piezo-phototronics.**

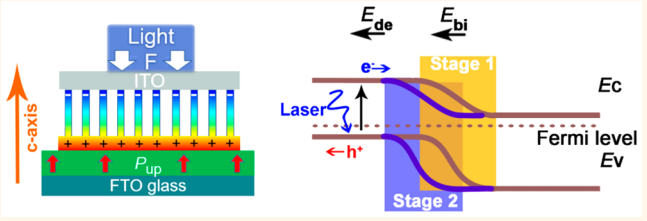

KEYWORDS: *piezo-phototronic effect, ferroelectricity, photovoltaic performances, ZnO nanowires, BLFO film*

In recent decades, global warming and energy crises have become increasingly severe. Considerable research has endeavored to explore green renewable energy.[1−4] Photoelectric energy conversion in ferroelectrics was proposed more than 30 years ago, which is receiving intense interest since it can be used for a direct conversion of light into electricity through a photovoltaic effect.[5−8] The photovoltaic effect usually involves two basic processes. First, the device absorbs incident photons to excite an electron−hole pair as a charge carrier. Subsequently, the driving force inside the photoelectric device transports carriers to the electrode. The polarization-induced depolarization field is usually considered as the driving force for charge carriers in ferroelectric materials.[9] A steady and vigorous driving force is a crucial factor in determining the photovoltaic performance for photoelectric devices. Among the ferroelectric materials, $BiFeO_3$ (BFO) has aroused great interest in the past few decades due to its visible-light photovoltaic effect, multiferroic properties at room temperature, and related potential applications. BFO films prepared by chemical solution deposition method have the advantages of low-cost and accurately control the chemical components. Although photovoltaic properties of BFO-based materials have been widely studied, exploring the coupling between ferroelectricity and other physical effects is of great significance to design and investigate high-performance optoelectronic devices with multifunctional characteristics.

Received: June 30, 2020
Accepted: August 7, 2020
Published: August 7, 2020

https://dx.doi.org/10.1021/acsnano.0c05398
ACS Nano 2020, 14, 10723−10732

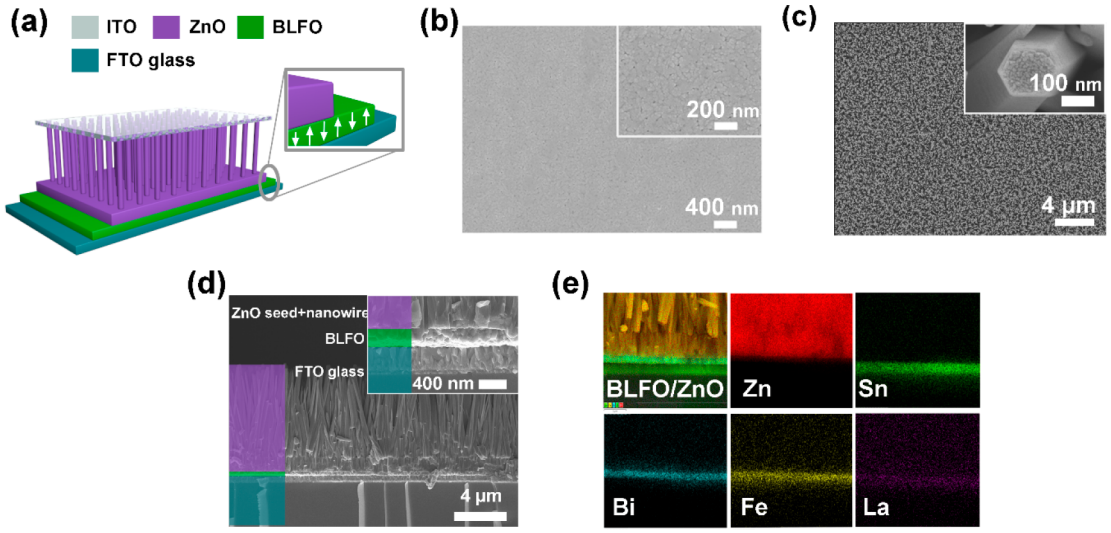

Figure 1. (a) Schematic structure of the BLFO/ZnO heterojunction. Top-view SEM images of the (b) BLFO film and (c) ZnO nanowire arrays, respectively. (d) Cross-section SEM image of the BLFO/ZnO heterojunction. Each inset (a–d) represents a locally enlarged view of the corresponding master graph. (e) EDS elemental maps for the interfaces of the heterojunction.

The piezo-phototronic effect, which is about the coupling among semiconductor, piezoelectric, and photoexcitation characteristics, can modulate the performance of photoelectric devices by tuning the transport process of the charge carriers, thereby establishing a field of research.[10−12] The piezo-phototronic effect is excited simply by applying a static mechanical strain without changing the device materials and structures. One-dimensional (1D) nanomaterials are excellent candidates for piezo-phototronics benefiting from their good mechanical endurance. ZnO as a piezoelectric semiconductor has been widely applied in areas such as sensors, nanoelectronics, and energy harvester owing to its mature preparation process and multifunctional materials characteristics.[13−15] At present, the piezo-phototronic effect based on ZnO nanostructures has been extensively used in solar cells, photodetectors, photocatalysis, neuromorphic computing, two-dimensional materials, and many other fields.[16−21]

Although the ferroelectricity-enhanced piezo-phototronic effects in V-doped ZnO nanosheets has been realized by introducing ferroelectricity and the piezo-phototronic effect, the modulation of photovoltaic performance of the device exerted by external electric field has not been investigated.[11] A high-performance photodetector has been achieved through the combination of piezo-phototronic and ferroelectric effects; however, photovoltaic properties under the concurrent stimulus of external strain and polarization has still been lacking.[22] On the other hand, from the viewpoint of material selection, photovoltaic performance of BFO/ZnO heterojunction has been examined; nevertheless, the influence of piezo-phototronic effect on the photovoltaic properties of BFO/ZnO heterojunction has not been investigated.[5,23] Therefore, the photovoltaic properties of devices under the simultaneous action of external strain and electric field are of considerable significance to examine the coupling between piezo-phototronic effect and ferroelectricity from the perspective of both industries and fundamental science community, which will widen the application range of piezo-phototronic effect.

In this study, we prepared a *p*-type La-doped $BiFeO_3$ ($Bi_{0.85}La_{0.15}FeO_3$, BLFO) film/*n*-type ZnO nanowire arrays heterojunction via the sol–gel and hydrothermal methods and then investigated the piezo-phototronic effect and ferroelectricity in modulating the photovoltaic properties of the heterojunction. The V_{OC} and J_{SC} of the BLFO/ZnO heterojunction are notably ameliorated by applying the compressive strain to modulate the charge carrier transport behavior using the piezo-phototronic effect, and the resulting changes in the energy band structure have also been verified by finite element analysis (FEA). Meanwhile, by introducing external electric field poling accompanying compressive strain, the direction of the depolarization field within a BLFO ferroelectric film can be switched to be consistent with the built-in field, which is equivalent to enhancing the total driving force of charge carriers, leading to the further improvement in the photovoltaic performance of the heterojunction. What is more interesting, this device exhibits faster response speed and excellent mechanical stability. Furthermore, the corresponding working mechanism of the ferroelectric polarization and piezo-phototronics in the photovoltaic BLFO/ZnO heterojunction is discussed by analysizing the energy band structure at the heterojunction, and thus, the driving force for the separation of photogenerated carriers was systematically clarified. This work clearly clarifies the coupling mechanism between the piezo-phototronic effect and ferroelectricity to adjust the photovoltaic performance of heterojunction, which provides an insightful guidance and a strategy for designing high-performance photoelectric devices.

RESULTS AND DISCUSSION

The three-dimensional structural schematic diagram of the as-fabricated FTO/BLFO/ZnO/ITO device is schematically illustrated in Figure 1a. The detailed preparation process is described in the Experimental Section. FTO and ITO serve as the bottom and top electrodes of the BLFO/ZnO heterojunction, respectively. The top-view scanning electron microscope (SEM) images of BLFO film and ZnO nanowire arrays are presented in Figure 1b,c. From Figure 1b and its inset, BLFO film exhibited a dense and smooth surface with granular structure. As seen from Figure 1c, ZnO nanowire arrays are uniformly distributed on the BLFO film. Moreover, the inset of Figure 1c demonstrates a hexagonal cross-section and columnar

https://dx.doi.org/10.1021/acsnano.0c05398
ACS Nano 2020, 14, 10723−10732

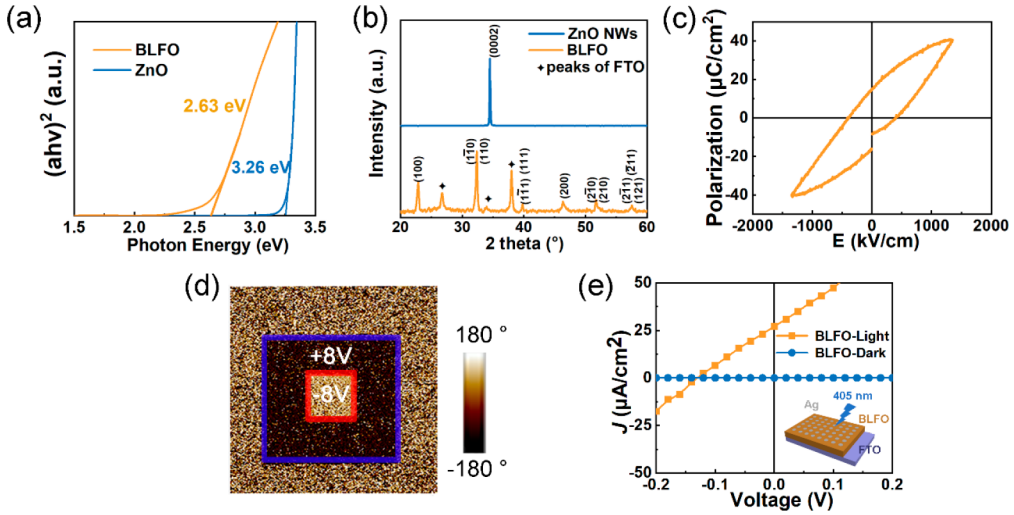

Figure 2. (a) Plot of $(\alpha h\nu)^2$ as a function of $h\nu$ of the BLFO film and ZnO nanowire arrays, respectively. (b) XRD pattern of BLFO film (orange) and ZnO nanowire arrays (blue). (c) Polarization hysteresis loops versus electric field of BLFO film. (d) Out-of-plane PFM phase image of the BLFO film. (e) $J-V$ curves of the BLFO film under the illumination of 405 nm wavelength at a power density of 100 mW/cm^2. The inset shows the diagrammatic sketch of experimental setup for testing the photovoltaic properties of BLFO film.

structure with average diameters of 190 nm, indicating the hexagonal wurtzite structure and highly *c*-axis orientation of ZnO nanowires.[15,24] Figure 1d gives the cross-section SEM image of the BLFO/ZnO heterojunction, from which the BLFO film of 270 nm thickness and the ZnO nanowires with length of 6 μm are unambiguously observed. It is worthwhile mentioning that the interface between BLFO film and ZnO nanowire arrays can be clearly identified from the inset in Figure 1d, which indicates each layer is well prepared and is of excellent crystallization. Moreover, as shown in Figure 1e, the energy-dispersive X-ray spectroscopy (EDS) maps for the interface of BLFO/ZnO demonstrate the distribution of necessary elements such as Bi, La, Sn and Zn, suggesting that the BLFO/ZnO sample with high chemical purity has been successfully prepared.

Next, the energy bandgaps (E_g) were measured and determined for the sake of analyzing photovoltaic properties of the BLFO/ZnO heterojunction. The transmission and absorbance spectra of the BLFO film and pure ZnO nanowire arrays synthesized on the FTO glass are plotted in Figure S2a and S2b, respectively. Obviously, the absorption of the BLFO is stronger than that of ZnO nanowires at near-ultraviolet waveband range. The energy bandgap can be deduced from the absorbance spectra using the Tauc equation[25,26]

$$(\alpha h\nu)^2 = A(h\nu - E_g) \quad (1)$$

where A, α, h, and ν are the constant, absorption coefficient, Planck constant, and light frequency, respectively. The E_g can be estimated from the optical absorption edge in Figure 2a. The corresponding calculated values of E_g for the BLFO film and ZnO are estimated to be ~2.63 and 3.26 eV, respectively. which are in good agreement with previous reports.[10,27,28] Consequently, the electron−hole pairs are mainly obtained in the BLFO film when the BLFO/ZnO heterojunction was irradiated by a 405 nm laser. In addition, the X-ray diffraction (XRD) spectra were measured to identify the composition of BLFO film and ZnO nanowires (Figure 2b), from which the reflection peaks of FTO substrate are labeled by a star. This figure shows that the reflection peaks of BLFO film (orange) are sharp, which indicates the BLFO film is of high quality with a polycrystalline nature. In addition, no peaks of secondary phases were detected within the diffractometer, meaning that the pure phase of BLFO has been favorably synthesized by the chemical solution deposition process. As can be seen in the Figure 2b for the pattern of ZnO nanowires (blue), only the (0002) diffraction peak at 2θ = 34.35° is observed, illustrating that the ZnO nanowires are *c*-axis oriented, which enables potential application for the piezo-phototronic effect in the BLFO/ZnO heterojunction.[12,14,15,29] To further understand the ferroelectric characteristics of BLFO films, the microscopic and macroscopic ferroelectric properties have been measured by piezoresponse force microscope (PFM) equipment and ferroelectric tester, respectively. As indicated from the polarization−electric ($P-E$) hysteresis loop of BLFO in Figure 2c, the remanent polarization (P_r) and coercive field (E_{co}) of BLFO film are about 18 μC/cm^2 and 400 kV/cm, respectively, which coincided with the previously reports.[30,31] We have also measured the $P-E$ hysteresis loop of the pure BFO film (Figure S3). It is universally accepted that La doping can improve ferroelectricity of $BiFeO_3$ by introducing structure distortion. That is to say, BLFO has better ferroelectricity than that of pure BFO.[32,33] Thus, we used BLFO to prepare heterojunction to conveniently study the effect of ferroelectricity on the photovoltaic performance of BLFO/ZnO heterojunction. Figure 2d presents the out-of-plane PFM phase image of the BLFO film, the central 3 × 3 μm^2 and 1 × 1 μm^2 regions were first polarized with the DC voltage amplitude of +8 and −8 V, respectively, and then the PFM phase was scanned with an AC probing voltage in the region of 5 × 5 μm^2 immediately. Obviously, the polarized central region exhibits a 180 deg phase difference, which indicates the BLFO film possesses local ferroelectric and electrically writable properties. The reversal polarization of the BLFO film corroborated by Figure 2d,e lays the foundation for the poling-tuned photovoltaic properties of the BLFO/ZnO heterojunction by an external electrical field. The current density−voltage ($J-V$) characteristics of the FTO/BLFO/Ag illuminated under 405 nm excitation wavelength at 100 mW/cm^2 laser power density are shown in Figure 2e. We also performed a $J-V$ measurement in the dark for a comparison and the inset in Figure 2e manifests a schematic diagram of the test setup for measuring the $J-V$ curves. As can be seen from Figure 2e, the V_{OC} and J_{SC} are about

https://dx.doi.org/10.1021/acsnano.0c05398
ACS Nano 2020, 14, 10723−10732

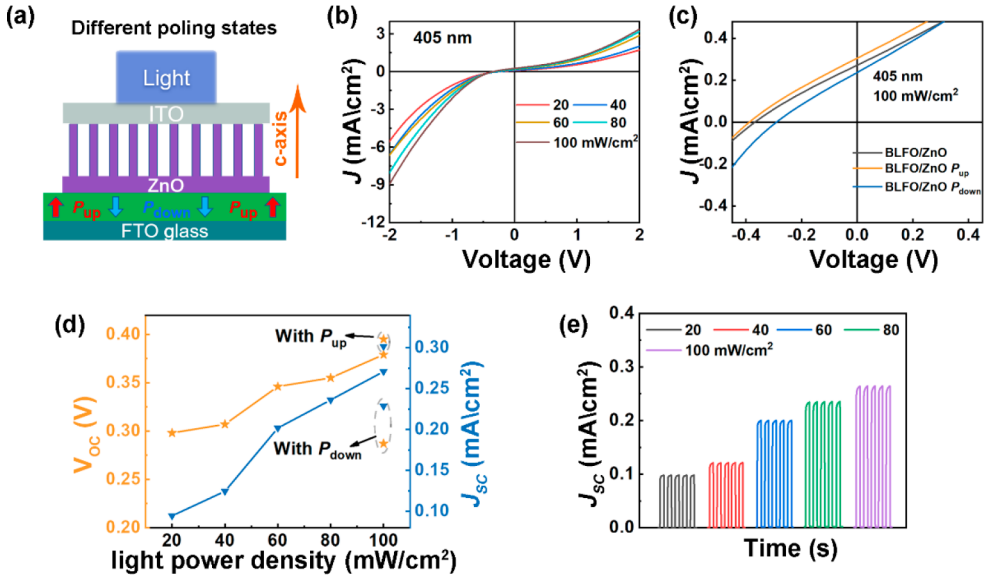

Figure 3. (a) Schematic diagram of the experimental setup for the BLFO/ZnO heterojunction with different poling states under 405 nm illumination. *J*−*V* curves of the BLFO/ZnO heterojunction (b) under different illumination power densities without poling and (c) under different poling states at 100 mW/cm^2 power light. (d) The dependence of J_{SC} and V_{OC} of the device on power density and poling state. (e) Time dependence of photocurrent under a zero bias for the device at different light power density.

0.14 V and 18 μA/cm^2, respectively. The *J*−*V* characteristics of the FTO/BLFO/Ag indicate the BLFO film has obviously photovoltaic effect, which could originate from the depolarization field inside the BLFO film. The depolarization field functions as a driving force for separating photogenerated charges carriers.[7,34,35]

Afterward, we tested the *J*−*V* characteristics of the BLFO/ZnO heterojunction under a series of laser power densities to verify its photovoltaic effect (Figure 3). Figure 3a shows a schematic diagram of the measured harness for photovoltaic properties with different poling states under 405 nm illumination, and the red and blue arrows inside the BLFO represent the upward and downward poling state, respectively. The *J*−*V* properties of the BLFO/ZnO under different illumination conditions were recorded and are shown in Figure 3b. Furthermore, we measured the photovoltaic properties of the BLFO/ZnO heterojunction with illumination after applying a 1 s pulse bias voltage of −10 V (upward poling) and +10 V (downward poling), respectively. Herein, the upward (downward) poling is defined when those heterojunctions are applied a negative (positive) pulse bias voltage on the top ITO transparent electrode. From Figure 3c, it is observed that the BLFO/ZnO heterojunction has various photovoltaic response parameters with regard to different poling states, which is related to the direction of the depolarization field in the BLFO film being opposite to the poling state. Thus, it will affect the carrier-transport behavior in the BLFO film.[7,26,36,37]

Figure 3d summarizes the J_{SC} and V_{OC} dependence on the illumination and poling states of the BLFO/ZnO heterojunction. Obviously, the photovoltaic properties of the BLFO/ZnO heterojunction are gradually enhanced with the increase of the laser power density. Compared with the photovoltaic properties irradiated at 100 mW/cm^2 light power density, the V_{OC} and J_{SC} increased by 4.2% and 11.3% under the upward poling state, respectively. These two parameters decreased by 24.3% and 15.6% under the downward poling state, respectively. Meanwhile, the repeatability of photovoltaic performance for the BLFO/ZnO heterojunction was tested at 0 V bias voltage by switching the 405 nm laser with various laser power densities (Figure 3e). A stable ON/OFF photocurrent density ratio makes usable as a photodetector. The results presented in Figure 3 imply reasonable structure design and excellent photovoltaic performance of the heterojunction, which provides a solid foundation investigation of the coupling mechanism between piezo-phototronic effect and ferroelectricity in the BLFO/ZnO NWs heterojunction.

The influence of external static compressive strain ranging from 0% to −2.3% on the electrical transportation of the BLFO/ZnO heterojunction was systematically explored, and the experimental results measured with laser illumination are summarized in Figure 4. The schematic map of the home-built experimental test platform was drawn and is shown in Figure S1. A piece of thin glass sheet was utilized to make the compressive strain evenly applied on the device and protect the device from possible damage by the tip of piezomotor.[38,39] Since the essence of the piezo-phototronic effect is to employ piezopotential to modulate the transport behaviors of photogenerated carriers, we measured the *J*−*V* curves at a light power density of 100 mW/cm^2 to better disclose the influence of piezo-phototronic effect on photovoltaic performance of the heterojunction. In addition, ZnO nanowire arrays in Figure 4a were filled with gradient colors, which represents the compressive strain has been applied to the device and the corresponding piezoelectric potential is generated within ZnO nanowires. As seen from Figure 4b, the photovoltaic response parameters of the device elevate with the increase of external static compressive strain. The V_{OC} and J_{SC} boosted from 0.379 V and 0.271 mA/cm^2 at free compressive strain to 0.397 V and 0.370 mA/cm^2 at −2.3% compressive strain, increased by 4.8% and 36.4%, respectively. The reason for the enhanced photovoltaic properties with the increase of compressive strain is that strain-induced piezopotential within ZnO promotes the separation and transportation of the charge carriers. The above-mentioned experimental results make it clear that piezo-phototronic effect can enhance the photovoltaic performance of the BLFO/ZnO heterojunction. Additionally, the J_{SC} of the BLFO/ZnO heterojunction under various external

https://dx.doi.org/10.1021/acsnano.0c05398
ACS Nano 2020, 14, 10723−10732

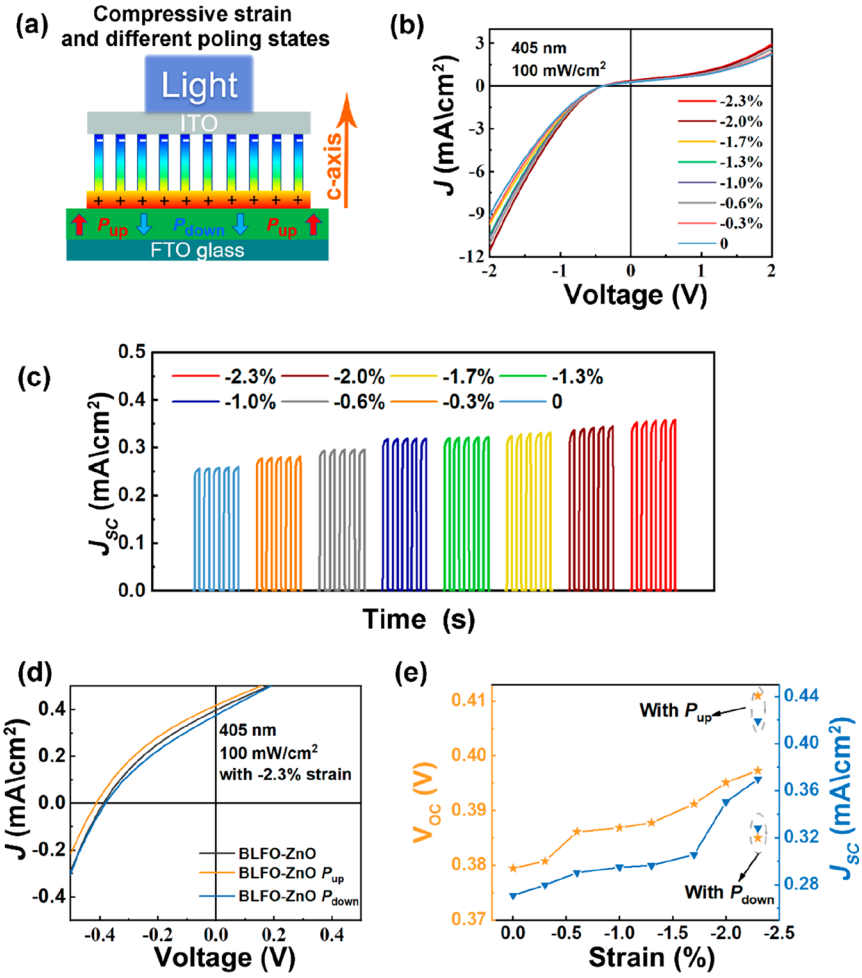

Figure 4. (a) Schematic diagram of the experimental setup for the BLFO/ZnO heterojunction under various compressive strain and different poling states. (b) $J-V$ curves of the BLFO/ZnO heterojunction under different compressive strain. (c) Time response and repeatability of the device under different compressive strain under 405 nm illumination. The illumination intensity is fixed at 100 mW/cm^2 in these cases. (d) $J-V$ curves of the BLFO/ZnO heterojunction under different poling states at −2.3% compressive strain. (e) The dependence of J_{SC} and V_{OC} of the device on compressive strain and poling state.

strain at 0 V bias voltage by switching the 405 nm laser with a fixed illumination of 100 mW/cm^2 were explored and recorded in Figure 4c. The J_{SC} exhibits an impressive repeatability under different external compressive strain, indicating the good mechanical durability of the device.

For the heterojunction composed of a ferroelectric film and piezoelectric semiconductor, it is indispensable to study the effect of ferroelectric polarization on the photovoltaic properties in order to investigate the coupling mechanism between piezo-phototronic effect and ferroelectric polarization. Figure 4d shows the $J-V$ properties of the BLFO/ZnO heterojunction measured under 405 nm illumination of 100 mW/cm^2 by simultaneously applying poling and compressive strain. The J_{SC} and V_{OC} of the BLFO/ZnO heterojunction without poling were observed to be 0.397 V and 0.370 mA/cm^2, respectively. Under upward poling, the corresponding values were boosted to 0.411 V and 0.419 mA/cm^2, while the corresponding values were decreased to 0.385 V and 0.328 mA/cm^2 under downward poling. Furthermore, the detailed variation tendency of the photovoltaic parameters versus external compressive strain is plotted in Figure 4e. Compared with the performance of the heterojunction without strain and poling, the J_{SC} and V_{OC} enhanced by 54.7% and 8.4% under applying −2.3% compressive strain and upward polarization, respectively, while under applying downward poling and −2.3% compressive strain, J_{SC} and V_{OC} merely increased by 21.1% and 1.6%, respectively. It is noted that the enhancement of the V_{OC} was weaker than that of J_{SC} under the same test conditions. According to the theory of semiconductor physics, the V_{OC} of a heterojunction is related to the quasi-Fermi levels of the junction, which is mainly dependent on the light intensity. Under ideal conditions, V_{OC} can be expressed by the Shockley equation[29,40]

$$V_{OC} = \frac{nkt}{q} \ln\left(\frac{J_{SC}}{J_S}\right) \tag{2}$$

where n, k, T, q, and J_S are the ideal factor, Boltzmann constant, absolute temperature and reverse saturation current density, respectively. This equation indicates the change in J_{SC} will have direct influences on V_{OC}. Through the derivation of the eq 2, the following equation can be obtained

$$d(V_{OC}) = \frac{nkt}{q} \frac{d(J_{SC})}{J_{SC}} \tag{3}$$

It can be seen that eq 3 clearly describe the changing relationship between V_{OC} and J_{SC}. Note that nkt/q is

https://dx.doi.org/10.1021/acsnano.0c05398
ACS Nano 2020, 14, 10723−10732

approximately 30 mV at room temperature.[29] Consequently, an increase of 100% in J_{SC} will lead to a boost of about 30 mV in V_{OC}. In other words, V_{OC} and J_{SC} satisfy weak positive correlation. From eq 2, it is deduced that J_{SC} will increase more obviously compared with V_{OC}, which is consistent with our experimental observation.

In order to further investigate the relationship between the piezo-phototronic effect and ferroelectricity, we compared the V_{OC} and J_{SC} for the BLFO/ZnO heterojunction under different testing conditions, as indicated in Table 1, from which the tunability of different test conditions is listed Table 2. From these two tables, it is easy to deduce that the modulation capability of photovoltaic properties of the heterojunction by compressive strain is larger than that under poling state. It has been reported that the driving force resulted from the electric field formed by piezoelectric charges is bigger than that by ferroelectric depolarization field, which can be used to explain the interesting experimental phenomena summarized in Tables 1 and 2.[5,41] More interestingly, as indicated from Table 2, the modulation capability under the synergistic action of the piezo-phototronic effect and ferroelectric polarization is higher than that under either piezo-phototronic effect or ferroelectric polarization. The tunability for E to A, B to A (E to D) and D to A (E to B) to is not a simple superposition correlation, which offers distinct testimony of mutually reinforce and synergistic coupling between the piezo-phototronic effect and ferroelectric polarization. When the device under the simultaneous action of upward poling state and compressive strain, both the change of energy band structure caused by compressive strain and the depolarization field within BLFO ferroelectric film will promote the transport behavior of photogenerated carriers.

Table 1. V_{OC} and J_{SC} for the BLFO/ZnO Heterojunction under Different Test Conditions

different test conditions	label	V_{OC} (V)	J_{SC} (mA/cm^2)
100 mW/cm^2	A	0.379	0.271
100 mW/cm^2 + P_{up}	B	0.395	0.302
100 mW/cm^2 + P_{down}	C	0.287	0.229
100 mW/cm^2 + −2.3% strain	D	0.397	0.370
100 mW/cm^2 + −2.3% strain + P_{up}	E	0.411	0.419
100 mW/cm^2 + −2.3% strain + P_{down}	F	0.385	0.328

The coupling of the piezo-phototronic effect and ferroelectricity can markedly enhance the photovoltaic properties of BLFO/ZnO heterostructure, which makes it useful in the field of photodetection. Rise and fall times are two crucial parameters for a photodetector, which are defined as the time interval between the normalized output current rising from 10% to 90% and falling from 90% to 10%, respectively. From Figure 5a, a rise time of 153.7 ms and a fall time of 108.8 ms under the strain-free condition without poling are obtained, respectively. By introducing the piezo-phototronic effect and ferroelectric polarization, a significantly improved response speed is achieved. The rise time and fall time decreases to 61.28 and 74.86 ms under concurrent −2.3% compressive strain and upward poling state, respectively. Besides, as indicated by Figure 5b, the time response of the BLFO/ZnO heterojunction under the −2.3% compressive and upward poling state presents excellent stability and repeatability. The J_{SC} of the heterojunction remains almost unchanged after 700 cycles. The significant enhancement of the photovoltaic properties and response speed of the BLFO/ZnO heterojunction under compressive strain and upward poling implies that the electric field derived from both compressive strain-induced positive piezo-charges and depolarization field within BLFO film can enhance the total driving force, which obviously promotes the velocity of separation and transport of the photogenerated carriers.

In order to further interpret the working mechanism of the synergistic coupling between the piezo-phototronic effect and ferroelectricity for the enhanced photovoltaic performance of the BLFO/ZnO heterojunction, FEA based on the COMSOL software is utilized to calculate the piezopotential distribution for ZnO nanowire arrays and then derive the energy band diagram of the BLFO/ZnO heterojunction under compressive strain, as revealed in Figure 6a and Figure S4. For simplification, the bottom surface of the ZnO nanowire arrays in Figure 6a is defined as zero potential and set as fixed constraint, and a vertical compressive force is applied on the top surface. Once a vertical compressive strain is applied along the $-c$ direction, negative (positive) piezo-charges would emerge immediately at $+c$ ($-c$) surface of the ZnO nanowires due to piezoelectric polarization effect, so the energy band structure of the BLFO/ZnO heterojunction alters correspondingly. The piezopotential for ZnO nanowires via FEA method provides an idea for constructing energy band of the BLFO/ZnO heterojunction by theoretical calculation with no poling with compressive strain.

Furthermore, the energy band diagrams of the device under different conditions are schematically depicted in Figure 6b−d. Generally, the BFO-based materials can act as ferroelectric semiconductors exhibited p-type conduction due to Bi volatilization.[9,42−45] The schematic energy band diagram of the BLFO/ZnO heterojunction at the initial state without compressive strain and the poling is shown in Figure S5. In this case, an original depletion (stage 1 in Figure 6b−d) zone and a build-in field (E_{bi}) of p−n junction are formed at the interface between BLFO and ZnO, from which the direction of the E_{bi} points from ZnO to BLFO. When the heterojunction is illuminated under a 405 nm laser, the incident light is mainly absorbed by the BLFO layer, thus generates the electron−hole pairs wherein. The photogenerated electron−hole pairs are swept to the back and surface sides of the heterojunction by the built-in field.

When a compressive strain and upward poling were simultaneously applied to the heterojunction, two things happened. One, the strain-induced negative/positive piezo-charges would appear at the $+c$ (top)/$-c$ (bottom) surface of the ZnO nanowires due to piezo-phototronic effect, respec-

Table 2. Tunability of Different Test Conditions According to the Data in Table 1

V_{OC}				J_{SC}			
P_{down} (%)	P_{up} (%)	−2.3% strain (%)	P_{up} + −2.3% strain (%)	P_{down} (%)	P_{up} (%)	−2.3% strain (%)	P_{up} + −2.3% train (%)
−24.3 (C to A)	4.2 (B to A)	4.8 (D to A)	8.4 (E to A)	−15.6 (C to A)	11.3 (B to A)	36.4 (D to A)	54.7 (E to A)
−3.1 (F to D)	3.4 (E to D)	4.1 (E to B)		−11.2 (F to D)	13.4 (E to D)	38.9 (E to B)	

https://dx.doi.org/10.1021/acsnano.0c05398
ACS Nano 2020, 14, 10723−10732

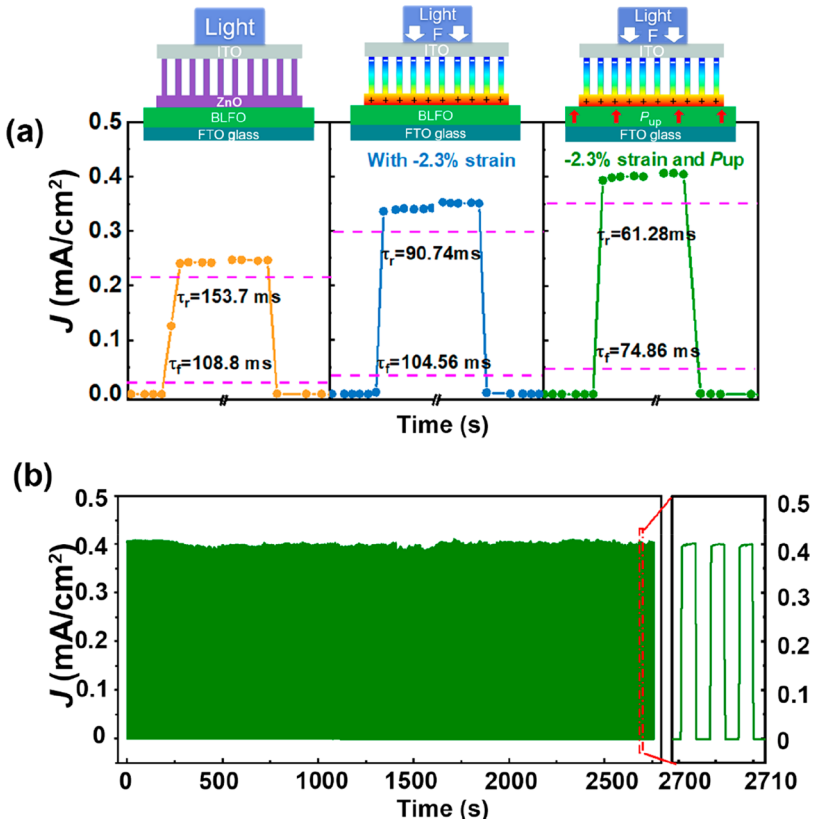

Figure 5. (a) Response time of the BLFO/ZnO heterojunction with different measurement conditions. (b) Durability test results of the BLFO/ZnO heterojunction with −2.3% compressive strain and upward poling state under the illumination of 405 nm and power density of 100 mW/cm^2.

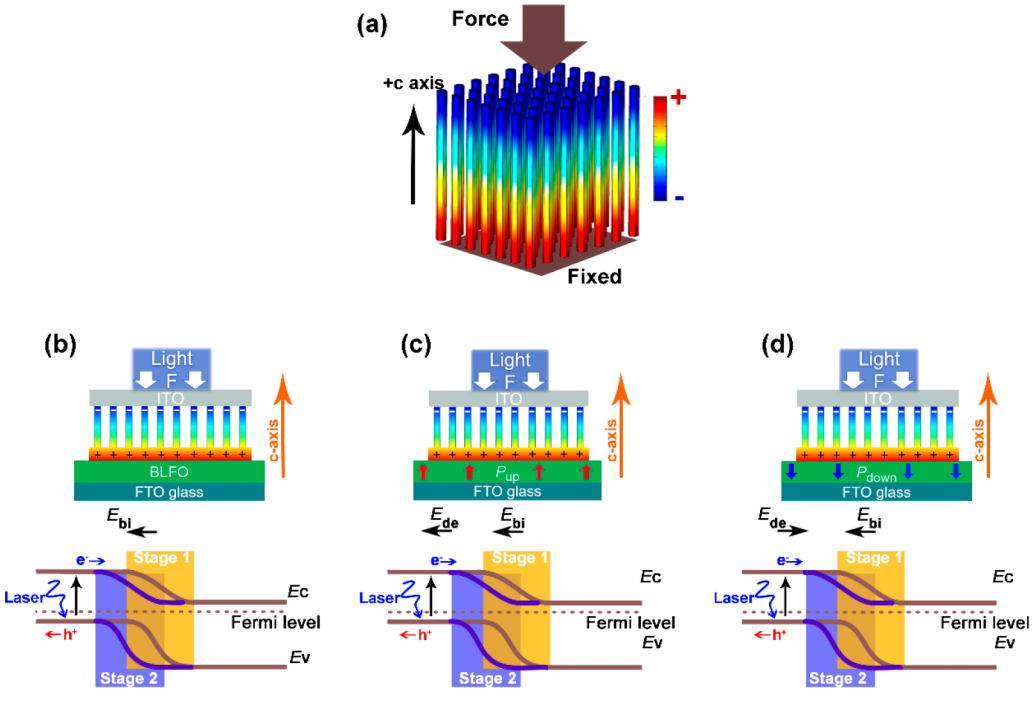

Figure 6. (a) FEA calculation results of the piezo-potential distributions in ZnO nanowire arrays. Schematic energy band diagrams of the BLFO/ZnO heterojunction under (b) compressive strain, (c) compressive strain with upward poling state, and (d) compressive strain and downward poling state.

tively.[12,14] The conduction band and valence band (E_c and E_v) at the p−n junction interface junction will lower locally (blue line in Figure 6b−d). Thus, the width of depletion zone increases in BLFO and decreases in ZnO. In other words, the depletion zone

https://dx.doi.org/10.1021/acsnano.0c05398
ACS Nano 2020, 14, 10723−10732

will shrink on the ZnO side and expand on the BLFO side, which is equivalent to the whole depletion zone shifts toward the BLFO side (stage 2 in Figure 6b–d).[46,47] Therefore, the effective voltage drop in the *p*-type depletion region increases under applied testing voltage, which enhances the separation efficiency of electron–hole pairs in the depletion region near BLFO.[36] Considering that the photogenerated electron–hole pairs are mainly produced at the *p*-type BLFO side, the photovoltaic properties and response speed of the BLFO/ZnO heterojunction can be improved via applied compressive strain.[46−49] In Figure S4, a one-dimensional model is employed to explore the influence of the externally compressive strain on the energy band of the heterojunction. The boundary condition of surface charge density is applied to the interface of the BLFO/ZnO to introduce the surface charge density of piezo-charges. The positive piezo-charges generated at the interface make the energy band lower locally (red line in Figure S4), this change lead to the variation of depletion region from the original state without strain (orange area) to the piezo-modulation state with compressive strain (blue area). The theoretical calculations in Figure 6a and Figure S4 match well with the physical mechanism proposed in Figure 6b–d.

On the other hand, the direction of the depolarization field (E_{de}) within BLFO film will be opposite to the poling direction when the BLFO film is poled by an external electric field. Herein, under the upward poling state, the direction of E_{de} within the BLFO film is consistent with that of the E_{bi} in the depletion zone of the heterojunction, making the total driving force of the photogenerated electron–hole pairs enhanced in the entire device, which further improves the efficiency of separation and transportation of photogenerated carriers (Figure 6c). Thus, under concurrent compressive strain and upward poling, the BLFO/ZnO heterojunction present superior photovoltaic properties than those by applying either compressive strain or the upward poling. On the contrary, the direction of E_{de} is opposite to that of E_{bi} when a compressive strain and downward poling act on the heterojunction simultaneously (Figure 6d), which decreases the total driving force of photogenerated carriers and thus reduce the photovoltaic performance of the heterojunction.

CONCLUSIONS

In summary, we successfully prepared the BLFO/ZnO heterojunction on the FTO substrate and have systematically investigated the coupling mechanism of the piezo-phototronic effect and ferroelectric polarization in the heterojunction. The heterojunction showed a significant enhancement in photovoltaic performance under 405 nm laser illumination. By applying a compressive strain and upward poling, the overall driving force of the photogenerated carriers is ameliorated, which notably promotes the separation and transport behavior of photogenerated carriers in the heterojunction. Compared with the photovoltaic performance of the heterojunction without strain and poling, the J_{SC} and V_{OC} enhanced by 54.7% and 8.4% by simultaneously applying −2.3% compressive strain and upward polarization, respectively. The reasonable schematical energy band diagrams are proposed to explain the working mechanism of the heterojunction under the synergistic effect of piezo-phototronic effect and ferroelectric polarization, which was partly validated by the theoretical calculation. This work not only offers a feasible and common approach for improving the heterojunction based on ferroelectric film by piezo-phototronic effect but also facilitates the development of human–machine interaction systems integrated with photoexcitation.

EXPERIMENTAL SECTION

Fabrication of BLFO and BFO Films. BLFO films were prepared via the sol–gel method and spin-coating technique. The precursor solution of BLFO was achieved by dissolving 1.3606 g of bismuth nitride [$Bi(NO_3)_3{\cdot}5H_2O$], 1.212 g of iron nitrate [$Fe(NO_3){\cdot}9H_2O$], and 0.1948 g of lanthanum nitrate [$La(NO_3)_3{\cdot}6H_2O$] in 4 mL of 2-methoxyethanol. Additionally, 2 mL of acetic acid and 3 mL of acetic anhydride were mixed in the solution as dehydrating agents, and the viscosity of the resulting solution was adjusted by adding 100 μL of ethanolamine. Finally, an appropriate amount of 2-methoxyethanol was added to obtain 10 mL of precursors with a solution concentration of 0.3 mol/L. The mixture was vigorously stirred for 12 h at room temperature to gain a stable and uniform solution. Subsequently, the above precursor solution was spin-coated on FTO conducting glass at 800 rpm initially for 10 s and then at 4000 rpm for 30 s in ambient conditions, followed by pyrolyzing at 350 °C for 5 min and then 600 °C for 20 min. The above process was replicated 5 times to obtain BLFO film with homogeneous thickness. The precursor solution of BFO was achieved by dissolving 1.6000 g of bismuth nitride [$Bi(NO_3)_3{\cdot}5H_2O$] and 1.2120 g of iron nitrate [$Fe(NO_3){\cdot}9H_2O$] in 4 mL of 2-methoxyethanol. The preparation process of the BFO film was the same as that for BLFO.

Fabrication of ZnO Nanowires. hexamethylenetetramine [$(CH_2)_6N_4$, HMTA] (0.7008 g) and zinc nitrate hexahydrate [$Zn(NO_3)_2{\cdot}6H_2O$] (2.9875 g) were mixed in 200 mL of deionized water to prepare a growth solution with a concentration of 0.05 mol/L. The ZnO seeds were deposited onto the BLFO film via a magnet sputtering system (JGP-350B) at a substrate temperature of 500 °C and then transferred into the growth solution at 90 °C for 9 h in a thermostat oven. Finally, the ITO-transparent conductive electrode with an area of 3 × 3 mm^2 was sputtered with magnetron sputtering on top of the ZnO nanowire arrays at 350 °C. The testing Cu wires were attached to the top and bottom electrodes by silver paste. A thin layer of Kapton tape was employed to fix the testing wires and improve the robustness. Finally, a thin glass sheet is placed on the upper part of the device to not only ensure evenly applied stress to the ZnO nanowire arrays but also protect the device from the piezomotor.

Characterization and Measurement. The crystal structure and surface morphology were studied by XRD (Bruker D8 Advance, Cu Ka radiation) and SEM (Carl Zeiss Geminisem500), respectively. Transmission and absorption spectra of BLFO film and ZnO nanowire arrays were measured by a UV–vis spectrophotometer (Varian Cary 5000) in a wavelength range of 300–800 nm. Sliver film electrodes with diameter of 0.5 mm were sputtered on the surface of BLFO films as the top electrodes to test the photovoltaic properties of the BLFO/ZnO heterojunction. Hysteresis loop measurement was performed by a ferroelectric tester (PolyK Technologies, PK-CPE901) at the frequency of 1 kHz. The mocroscopic ferroelectric properties of the BLFO film was measured with a PFM (Multimode 8, Bruker). The homemade test platform was constructed with the piezomotor (P-753.3CD, PI company), Keithley 2400 source meter, XYZ linear translation stage (movement resolution of 10 μm), 405 nm laser source, probe station, and a computer equipped with measurement software, as shown in Figure S1. Among them, the piezomotor can provide nanoscale displacement to ensure the precise exertion of compressive strain during the test process. The laser power density was measured and calibrated by a power meter (CEL-FZ-A, AuLight). A 10 V DC voltage was applied to the device for 1 s to pole the BLFO film. All of the measurements were carried out at room temperature.

ASSOCIATED CONTENT

Supporting Information

The Supporting Information is available free of charge at https://pubs.acs.org/doi/10.1021/acsnano.0c05398.

https://dx.doi.org/10.1021/acsnano.0c05398
ACS Nano 2020, 14, 10723−10732

Schematic diagram of homemade experimental platform; UV−vis transmission spectra and absorption spectra of the BLFO film and ZnO nanowire arrays; polarization hysteresis loops versus electric field of BFO film; calculation of the external compressive strain influence on the energy band diagrams for BLFO/ZnO heterojunction; schematic energy band diagrams of the BLFO/ZnO heterojunction at an initial stage without compressive strain and poling (PDF)

AUTHOR INFORMATION

Corresponding Authors

Haiwu Zheng − *International Joint Research Laboratory of New Energy Materials and Devices of Henan Province, School of Physics and Electronics, Henan University, Kaifeng 475004, P.R. China;* orcid.org/0000-0002-2021-4159; Email: zhenghaiw@ustc.edu

Xingfu Wang − *Institute of Semiconductor Science and Technology, South China Normal University, Guangzhou 510631, P.R. China;* orcid.org/0000-0001-7450-6723; Email: xfwang@scnu.edu.cn

Zhong Lin Wang − *Beijing Institute of Nanoenergy and Nanosystems Chinese Academy of Sciences, Beijing 100083, P.R. China; School of Materials Science and Engineering, Georgia Institute of Technology, Atlanta, Georgia 30332-0245, United States;* orcid.org/0000-0002-5530-0380; Email: zhong.wang@mse.gatech.edu

Authors

Yuanzheng Zhang − *International Joint Research Laboratory of New Energy Materials and Devices of Henan Province, School of Physics and Electronics, Henan University, Kaifeng 475004, P.R. China*

Liya Yang − *International Joint Research Laboratory of New Energy Materials and Devices of Henan Province, School of Physics and Electronics, Henan University, Kaifeng 475004, P.R. China*

Yaju Zhang − *International Joint Research Laboratory of New Energy Materials and Devices of Henan Province, School of Physics and Electronics, Henan University, Kaifeng 475004, P.R. China*

Zhenyu Ding − *International Joint Research Laboratory of New Energy Materials and Devices of Henan Province, School of Physics and Electronics, Henan University, Kaifeng 475004, P.R. China*

Mengjun Wu − *International Joint Research Laboratory of New Energy Materials and Devices of Henan Province, School of Physics and Electronics, Henan University, Kaifeng 475004, P.R. China*

Yan Zhou − *International Joint Research Laboratory of New Energy Materials and Devices of Henan Province, School of Physics and Electronics, Henan University, Kaifeng 475004, P.R. China*

Chunli Diao − *International Joint Research Laboratory of New Energy Materials and Devices of Henan Province, School of Physics and Electronics, Henan University, Kaifeng 475004, P.R. China*

Complete contact information is available at: https://pubs.acs.org/10.1021/acsnano.0c05398

Author Contributions

⊥These authors contributed equally to this work.

Notes

The authors declare no competing financial interest.

ACKNOWLEDGMENTS

The authors gratefully acknowledge support from the National Key Research and Development of China (Grant No. 2016YFA0202704), the National Natural Science Foundation of China (Nos. 51872074, 11804103 and 51432005), the Program for Innovative Research Team in Science and Technology in University of Henan Province (19IRTSTHN019), and first-class discipline cultivation project of Henan University(2019YLZDJL06, 2019YLZDYJ04). We express sincere gratitude to Prof. Guoliang Yuan and Dr. Candidate Zhongshuai Xie for the PFM characterization and helpful discussions.

REFERENCES

(1) Shi, L.; Bucknall, M. P.; Young, T. L.; Zhang, M.; Hu, L.; Bing, J.; Lee, D. S.; Kim, J.; Wu, T.; Takamure, N.; McKenzie, D. R.; Huang, S.; Green, M. A.; Ho-Baillie, A. W. Y. Gas Chromatography−Mass Spectrometry Analyses of Encapsulated Stable Perovskite Solar Cells. *Science* **2020**, *368*, eaba2412.

(2) Im, H.; Kim, T.; Song, H.; Choi, J.; Park, J. S.; Ovalle-Robles, R.; Yang, H. D.; Kihm, K. D.; Baughman, R. H.; Lee, H. H.; Kang, T. J.; Kim, Y. H. High-Efficiency Electrochemical Thermal Energy Harvester Using Carbon Nanotube Aerogel Sheet Electrodes. *Nat. Commun.* **2016**, *7*, 10600.

(3) Wu, M.; Zheng, T.; Zheng, H.; Li, J.; Wang, W.; Zhu, M.; Li, F.; Yue, G.; Gu, Y.; Wu, J. High-Performance Piezoelectric-Energy-Harvester and Self-Powered Mechanosensing Using Lead-Free Potassium−Sodium Niobate Flexible Piezoelectric Composites. *J. Mater. Chem. A* **2018**, *6*, 16439−16449.

(4) Zhang, Y.; Wu, M.; Zhu, Q.; Wang, F.; Su, H.; Li, H.; Diao, C.; Zheng, H.; Wu, Y.; Wang, Z. L. Performance Enhancement of Flexible Piezoelectric Nanogenerator *via* Doping and Rational 3D Structure Design for Self-Powered Mechanosensational System. *Adv. Funct. Mater.* **2019**, *29*, 1904259.

(5) Fan, Z.; Yao, K.; Wang, J. Photovoltaic Effect in an Indium-Tin-Oxide/Zno/$BiFeO_3$/Pt Heterostructure. *Appl. Phys. Lett.* **2014**, *105*, 162903.

(6) Ji, Y.; Gao, T.; Wang, Z. L.; Yang, Y. Configuration Design of $BiFeO_3$ Photovoltaic Devices for Self-Powered Electronic Watch. *Nano Energy* **2019**, *64*, 103909.

(7) Wurfel, P.; Batra, I. P. Depolarization-Field-Induced Instability in Thin Ferroelectric Films—Experiment and Theory. *Phys. Rev. B* **1973**, *8*, 5126−5133.

(8) Choi, T.; Lee, S.; Choi, Y. J.; Kiryukhin, V.; Cheong, S.-W. Switchable Ferroelectric Diode and Photovoltaic Effect in $BiFeO_3$. *Science* **2009**, *324*, 63−65.

(9) Zhao, R.; Ma, N.; Song, K.; Yang, Y. Boosting Photocurrent *via* Heating $BiFeO_3$ Materials for Enhanced Self-Powered UV Photodetectors. *Adv. Funct. Mater.* **2020**, *30*, 1906232.

(10) Duan, Y.; Cong, M.; Jiang, D.; Zhang, W.; Yang, X.; Shan, C.; Zhou, X.; li, M.; Li, Q. ZnO Thin Film Flexible UV Photodetectors: Regulation on the ZnO/Au Interface by Piezo-Phototronic Effect and Performance Outcomes. *Adv. Mater. Interfaces* **2019**, *6*, 1900470.

(11) Dai, Y.; Wu, C.; Wu, Z.; Zhao, Z.; Li, L.; Lu, Y.; Wang, Z. L. Ferroelectricity-Enhanced Piezo-Phototronic Effect in 2D V-Doped ZnO Nanosheets. *Adv. Sci.* **2019**, *6*, 1900314.

(12) Pan, Z.; Peng, W.; Li, F.; He, Y. Carrier Concentration-Dependent Piezotronic and Piezo-Phototronic Effects in ZnO Thin-Film Transistor. *Nano Energy* **2018**, *49*, 529−537.

(13) Su, Y.; Gupta, K.; Hsiao, Y.; Wang, R.; Liu, C. Gigantic Enhancement of Electricity Generation in Piezoelectric Semiconductors by Creating Pores as a Universal Approach. *Energy Environ. Sci.* **2019**, *12*, 410−417.

(14) Qiao, S.; Liu, J.; Fu, G.; Ren, K.; Li, Z.; Wang, S.; Pan, C. Zno Nanowire Based Cigs Solar Cell and Its Efficiency Enhancement by the Piezo-Phototronic Effect. *Nano Energy* **2018**, *49*, 508−514.
(15) Qiao, S.; Liu, J.; Niu, X.; Liang, B.; Fu, G.; Li, Z.; Wang, S.; Ren, K.; Pan, C. Piezophototronic Effect Enhanced Photoresponse of the Flexible Cu(In,Ga)Se_2 (CIGS) Heterojunction Photodetectors. *Adv. Funct. Mater.* **2018**, *28*, 1707311.
(16) Kumar, B.; Kim, S.-W. Energy Harvesting Based on Semiconducting Piezoelectric ZnO Nanostructures. *Nano Energy* **2012**, *1*, 342−355.
(17) Ou, C.; Sanchez-Jimenez, P. E.; Datta, A.; Boughey, F. L.; Whiter, R. A.; Sahonta, S. L.; Kar-Narayan, S. Template-Assisted Hydrothermal Growth of Aligned Zinc Oxide Nanowires for Piezoelectric Energy Harvesting Applications. *ACS Appl. Mater. Interfaces* **2016**, *8*, 13678−13683.
(18) Pan, L.; Sun, S.; Chen, Y.; Wang, P.; Wang, J.; Zhang, X.; Zou, J. J.; Wang, Z. L. Advances in Piezo-Phototronic Effect Enhanced Photocatalysis and Photoelectrocatalysis. *Adv. Energy Mater.* **2020**, *10*, 2000214.
(19) Nie, J.; Zhang, Y.; Li, L.; Wang, J. Piezo-Phototronic Effect Enhanced Photodetectors Based on $MAPbI_3$ Perovskite. *J. Mater. Chem. C* **2020**, *8*, 2709−2718.
(20) Kumar, M.; Kim, J.; Wong, C.-P. Transparent and Flexible Photonic Artificial Synapse with Piezo-Phototronic Modulator: Versatile Memory Capability and Higher Order Learning Algorithm. *Nano Energy* **2019**, *63*, 103843.
(21) Wu, W.; Wang, L.; Li, Y.; Zhang, F.; Lin, L.; Niu, S.; Chenet, D.; Zhang, X.; Hao, Y.; Heinz, T. F.; Hone, J.; Wang, Z. L. Piezoelectricity of Single-Atomic-Layer MoS_2 for Energy Conversion and Piezotronics. *Nature* **2014**, *514*, 470−474.
(22) Shen, T.; Chu, Y.; Liao, Y.; Lee, W.; Kuo, H.; Lin, T.; Chen, Y. Ultrahigh-Performance Self-Powered Flexible Photodetector Driven From Photogating, Piezo-Phototronic, and Ferroelectric Effects. *Adv. Opt. Mater.* **2020**, *8*, 1901334.
(23) Katayama, T.; Sakamoto, W.; Yuitoo, I.; Takeuchi, T.; Hayashi, K.; Yogo, T. Enhancement of Photoinduced Electrical Properties of Al-Doped ZnO/$BiFeO_3$ Layered Thin Films Prepared by Chemical Solution Deposition. *Jpn. J. Appl. Phys.* **2015**, *54*, 10NA05.
(24) Bhatia, D.; Roy, S.; Nawaz, S.; Meena, R. S.; Palkar, V. R. Room Temperature Electrical Properties of $Bi_{0.7}Dy_{0.3}FeO_3$ Thin Films Deposited by PLD on ZnO Films for Potential Applications. *Microelectron. Eng.* **2016**, *163*, 60−66.
(25) Zhang, Y.; Zheng, H.; Wang, X.; Li, H.; Wu, Y.; Zhang, Y.; Su, H.; Yuan, G. Enhanced Photovoltaic Properties of Gradient Calcium-Doped $BiFeO_3$ Films. *Ceram. Int.* **2020**, *46*, 10083−10088.
(26) Zhu, M.; Zheng, H.; Zhang, J.; Yuan, G.; Wang, K.; Yue, G.; Li, F.; Chen, Y.; Wu, M.; Zhang, W. Polarization Dependent Ferroelectric Photovoltaic Effects in BFTO/CuO Thin Films. *Appl. Phys. Lett.* **2017**, *111*, 032901.
(27) Zheng, P.; Sun, B.; Chen, Y.; Elshekh, H.; Yu, T.; Mao, S.; Zhu, S.; Wang, H.; Zhao, Y.; Yu, Z. Photo-Induced Negative Differential Resistance in a Resistive Switching Memory Device Based on $BiFeO_3$/ZnO Heterojunctions. *Appl. Mater. Today* **2019**, *14*, 21−28.
(28) Li, F.; Zheng, H.; Zhu, M.; Zhang, X.; Yuan, G.; Xie, Z.; Li, X.; Yue, G.; Zhang, W. Photovoltaic Enhancement by Au Surface-Plasmon Effect for La Doped $BiFeO_3$ Films. *J. Mater. Chem. C* **2017**, *5*, 10615−10623.
(29) Sun, J.; Hua, Q.; Zhou, R.; Li, D.; Guo, W.; Li, X.; Hu, G.; Shan, C.; Meng, Q.; Dong, L.; Pan, C.; Wang, Z. L. Piezo-Phototronic Effect Enhanced Efficient Flexible Perovskite Solar Cells. *ACS Nano* **2019**, *13*, 4507−4513.
(30) Yang, K.; Yang, S.; Zhang, Y. Ferroelectric Properties in Multiferroic $BiFeO_3$Thin Films Codoped with La and Co. *Ferroelectrics* **2010**, *410*, 63−68.
(31) Zhang, S.; Zhang, Y.; Lu, M.; Du, C.; Chen, Y.; Liu, Z.; Zhu, Y.; Ming, N. Substitution-Induced Phase Transition and Enhanced Multiferroic Properties of $Bi_{1-x}La_xFeO_3$ Ceramics. *Appl. Phys. Lett.* **2006**, *88*, 162901.
(32) Lee, J.-H.; Choi, H. J.; Lee, D.; Kim, M. G.; Bark, C. W.; Ryu, S.; Oak, M.-A.; Jang, H. M. Variations of Ferroelectric Off-Centering Distortion and *3d-4p* Orbital Mixing in La-Doped $BiFeO_3$ Multiferroics. *Phys. Rev. B: Condens. Matter Mater. Phys.* **2010**, *82*, 045113−045121.
(33) Yan, F.; Zhu, T.; Lai, M.; Lu, L. Enhanced Multiferroic Properties and Domain Structure of La-Doped. *Scr. Mater.* **2010**, *63*, 780−783.
(34) Qin, M.; Yao, K.; Liang, Y. C. Photovoltaic Mechanisms in Ferroelectric Thin Films with the Effects of the Electrodes and Interfaces. *Appl. Phys. Lett.* **2009**, *95*, 022912.
(35) Kim, D. J.; Jo, J. Y.; Kim, Y. S.; Chang, Y. J.; Lee, J. S.; Yoon, J.-G.; Song, T. K.; Noh, T. W. Polarization Relaxation Induced by Depolarization Field in Ultrathin Ferroelectric $BaTiO_3$ Capacitors. *Phys. Rev. Lett.* **2005**, *95*, 237602.
(36) Cao, J.; Chung, D. D. L. Electric Polarization and Depolarization in Cement-Based Materials, Studied by Apparent Electrical Resistance Measurement. *Cem. Concr. Res.* **2004**, *34*, 481−485.
(37) Wang, K.; Zheng, H.; Li, X.; Yuan, G.; Gao, W.; Wei, L.; Zhang, X.; Zhang, W. Effect of Top Electrodes and Light Sources on Photovoltaic Properties of Polycrystalline $Bi_4Ti_3O_{12}$ Film. *Mater. Lett.* **2016**, *179*, 182−185.
(38) Dai, Y.; Wang, X.; Peng, W.; Zou, H.; Yu, R.; Ding, Y.; Wu, C.; Wang, Z. L. Largely Improved Near-Infrared Silicon-Photosensing by the Piezo-Phototronic Effect. *ACS Nano* **2017**, *11*, 7118−7125.
(39) Pan, Z.; Peng, W.; Li, F.; He, Y. Piezo-Phototronic Effect on Performance Enhancement of Anisotype and Isotype Heterojunction Photodiodes. *Adv. Funct. Mater.* **2018**, *28*, 1706897.
(40) Zhang, Y.; Cui, W.; Zhu, Y.; Zu, F.; Liao, L.; Lee, S.-T.; Sun, B. High Efficiency Hybrid PEDOT:PSS/Nanostructured Silicon Schottky Junction Solar Cells by Doping-Free Rear Contact. *Energy Environ. Sci.* **2015**, *8*, 297−302.
(41) Zhang, Y.; Liu, Y.; Wang, Z. L. Fundamental Theory of Piezotronics. *Adv. Mater.* **2011**, *23*, 3004−3013.
(42) Kim, T.; Jeon, B.; Min, T.; Yang, S.; Lee, D.; Kim, Y.; Baek, S.; Saenrang, W.; Eom, C.; Song, T.; Yoon, J.; Noh, T. Continuous Control of Charge Transport in Bi-Deficient $BiFeO_3$ Films through Local Ferroelectric Switching. *Adv. Funct. Mater.* **2012**, *22*, 4962−4968.
(43) Tsurumaki, A.; Yamada, H.; Sawa, A. Impact of Bi Deficiencies on Ferroelectric Resistive Switching Characteristics Observed at *p*-Type Schottky-Like Pt/$Bi_{1-\delta}FeO_3$ Interfaces. *Adv. Funct. Mater.* **2012**, *22*, 1040−1047.
(44) Tsurumaki-Fukuchi, A.; Yamada, H.; Sawa, A. Resistive Switching Artificially Induced in a Dielectric/Ferroelectric Composite Diode. *Appl. Phys. Lett.* **2013**, *103*, 152903.
(45) Li, D.; Zheng, W.; Zheng, D.; Gong, J.; Wang, L.; Jin, C.; Li, P.; Bai, H. Magnetization and Resistance Switchings Induced by Electric Field in Epitaxial Mn:ZnO/$BiFeO_3$ Multiferroic Heterostructures at Room Temperature. *ACS Appl. Mater. Interfaces* **2016**, *8*, 3977−3984.
(46) Lin, P.; Pan, C.; Wang, Z. L. Two-Dimensional Nanomaterials for Novel Piezotronics and Piezophototronics. *Mater. Today Nano* **2018**, *4*, 17−31.
(47) Zou, H.; Li, X.; Peng, W.; Wu, W.; Yu, R.; Wu, C.; Ding, W.; Hu, F.; Liu, R.; Zi, Y.; Wang, Z. L. Piezo-Phototronic Effect on Selective Electron or Hole Transport through Depletion Region of Vis-NIR Broadband Photodiode. *Adv. Mater.* **2017**, *29*, 1701412.
(48) Wu, W.; Wang, Z. L. Piezotronics and Piezo-Phototronics for Adaptive Electronics and Optoelectronics. *Nat. Rev. Mater.* **2016**, *1*, 1.
(49) Liu, Y.; Niu, S.; Yang, Q.; Klein, B. D.; Zhou, Y. S.; Wang, Z. L. Theoretical Study of Piezo-Phototronic Nano-LEDs. *Adv. Mater.* **2014**, *26*, 7209−7216.

https://dx.doi.org/10.1021/acsnano.0c05398
ACS Nano 2020, 14, 10723−10732